JGR Oceans

RESEARCH ARTICLE

10.1029/2025JC022886

Detection of Satellite Sea Surface Temperature Extremes: Low Frequency Variability and Climate Change

F. Serva[1], S. Marullo[1], R. Iacono[2], E. Napolitano[2], V. de Toma[1], A. Landolfi[1], E. Organelli[1], A. Pisano[1], and R. Santoleri[1]

[1]Consiglio Nazionale delle Ricerche (CNR), Istituto di Scienze Marine (ISMAR), Rome, Italy, [2]Agenzia Nazionale per Le Nuove Tecnologie, l'Energia e lo Sviluppo Economico Sostenibile (ENEA), Frascati/Rome, Italy

Key Points:

- Detection of SST extremes (and their characteristics) depend on the algorithmic setup and observational data set
- Nonlinear detrending allows us to determine regions dominated by interannual and shorter variability
- Spurious MHW events are detected in the CCI data set during the early satellite era

Supporting Information:

Supporting Information may be found in the online version of this article.

Correspondence to:

F. Serva,
federico.serva@terrarum.eu;
federico.serva@artov.ismar.cnr.it

Citation:

Serva, F., Marullo, S., Iacono, R., Napolitano, E., de Toma, V., Landolfi, A., et al. (2025). Detection of satellite sea surface temperature extremes: Low frequency variability and climate change. *Journal of Geophysical Research: Oceans*, *130*, e2025JC022886. https://doi.org/10.1029/2025JC022886

Received 16 MAY 2025
Accepted 30 SEP 2025

Author Contributions:

Conceptualization: F. Serva, S. Marullo, R. Iacono, R. Santoleri
Data curation: F. Serva, A. Pisano
Formal analysis: F. Serva
Funding acquisition: R. Santoleri
Investigation: F. Serva
Methodology: F. Serva, S. Marullo, R. Iacono, R. Santoleri
Project administration: A. Landolfi, E. Organelli, A. Pisano, R. Santoleri
Software: F. Serva, S. Marullo
Supervision: R. Santoleri
Validation: F. Serva, S. Marullo, R. Iacono
Visualization: F. Serva
Writing – original draft: F. Serva

Abstract The occurrence of sea surface temperature (SST) extremes may provoke profound impacts on ocean health. In the last decade, much effort has been dedicated to understanding and systematically describing marine heatwaves (MHWs) and cold spells (MCSs), defined as prolonged periods of anomalously warm or cold SSTs at a given location, respectively. However, an objective and agreed detection criterion for such extremes, applicable to past and future climates alike and separating the effects of climate variability and change, is still missing. Analysis of four decades of global daily satellite-based SST data show that the identification of extremes is strongly dependent on the chosen data set and algorithmic choices that are difficult to set objectively. Sensitivity to the reference period (baseline) occurs because the warming trend shifts SST anomalies away from the baseline, resulting in a global increase in MHWs (moderate and strong) and a decrease in MCSs (strong and extreme). Here we show that the contributions from climate change can be effectively isolated by applying a data-driven approach based on the singular spectrum analysis, which, unlike linear detrending, does not assume a prescribed behavior for the trend. Detrending removes long-term changes in the occurrence of SST extremes, and also affects the metrics (such as intensity and duration) widely used to characterize these events. Data set intercomparison reveals possibly spurious MHW events in the early 1980s and quantitative discrepancies in the representation of long-term variability.

Plain Language Summary Prolonged periods of anomalously warm or cold sea surface temperatures are tied to weather systems and may impact ecosystem functioning. Many previous studies analyzed these extreme events in detail, including their effects and drivers, but their definition remains somehow contentious because of the non-stationarity of our warming climate system, and of the uncertainties related to the choice of a reference period. In this work we propose a methodology to isolate the effects of a warming background in the detection of sea surface temperature extremes, by means of a rigorous statistical technique. We find that the contribution of global warming varies spatially, and that the role of climate variability is dominant in regions such as the tropical Pacific Ocean. As found in previous works, overall warming leads to more frequent warm and rarer cold extremes at the global scale.

1. Introduction

Interest in marine temperature extremes has considerably increased during the last decades largely motivated by the impacts that these events have on ecosystem structure and functions, and human activities at sea (Smith et al., 2021). Marine heatwaves (MHWs) and marine cold spell (MCSs) are extended periods of anomalously warm or cold sea SSTs compared to a reference baseline, respectively. Operationally, a MHW/MCS is identified when SST exceeds (i.e., gets above/below, respectively) a percentile-based threshold of the historical SST distribution at a specific location for a certain number of consecutive days (A. J. Hobday et al., 2016; A. Hobday et al., 2018; Schlegel et al., 2021). This definition is meant to provide a simple and useful framework for quantifying and studying extreme temperature events in the ocean, allowing researchers to understand their occurrence, dynamics, and impacts on marine ecosystems, and policymakers to define mitigation strategies to adapt to these changes (Kajtar et al., 2024).

The definition of these extremes thus requires the definition of a suitable reference period for calculating a normal state, that is, the reference baseline or climatology, which is typically set as a 30-year period according to A. J. Hobday et al. (2016) and to the recommendations of the World Meteorological Organization (WMO). However, it has been noted that the definition of extremes based on climatological percentile thresholds, such as MHW and

Writing – review & editing: F. Serva, S. Marullo, R. Iacono, E. Napolitano, V. de Toma, A. Landolfi, E. Organelli, A. Pisano, R. Santoleri

MCS, is highly sensitive to the choice of the reference baseline (Thomas et al., 2023). This consideration becomes even more significant in the context of the ongoing global warming, which is gradually shifting average temperature conditions over time. In practice, if the reference baseline remains fixed, the temperature record will increasingly deviate from climatological values due to the long-term warming trend. This warming effect (Xu et al., 2022) results in increasing the occurrence and intensity of these extremes (Frölicher et al., 2018; Marullo et al., 2023; E. C. Oliver et al., 2021), possibly leading to a permanent MHW status in the future (Anav et al., 2024; Tanaka & Houtan, 2022). Several methods have been proposed to circumvent this problem, such as using a shifting baseline (Chiswell, 2022) or detrending the data prior to analysis (Ciappa, 2022; Martínez et al., 2023), or by adopting dynamical thresholds (Kashkooli et al., 2025; Smith et al., 2024). For observed data, linear detrending is widely used to evaluate whether anthropogenic trends influenced the occurrence of MHW events (Capotondi et al., 2024). Because of the relative shortness of the observational record, which spans four decades, it is anyway not easy to diagnose the contribution of internal and forced variability (L. Dong et al., 2024). To this end, model outputs or extended SST reconstructions have also been used (E. C. J. Oliver et al., 2018; Pilo et al., 2019), but such data are less reliable and/or comprehensive than satellite measurements.

Although a general consensus on the choice of the baseline remains elusive, there is a broad interest to separate the long-term warming trend when identifying extreme events, aligning with the basic idea that a MHW/MCS should denote a transient and abrupt anomaly relative to the expected local conditions in a given location. Trend removal helps re-establishing stationarity of local conditions, which are otherwise subject to changes due to global warming. Additionally, the appropriate algorithmic parameters choices (i.e., percentile threshold and minimum duration) might depend on the application of interest since ecological and biological responses can be diverse and complex (M. Li et al., 2024; Lubitz et al., 2024; Smith et al., 2023). For example, fixed temperature thresholds have been identified from the upper thermal limit of specific marine organisms, that is, the temperatures above which biological functions become impaired. This approach assumes that physiological limits are well adapted to the local conditions. However, at ecosystem level, where different ecosystem functions might have diverse temperature sensitivities, moving thresholds (percentile based) could be more appropriate (Gruber et al., 2021).

Furthermore, the statistical methodology does not disclose the role of the main drivers and/or processes responsible for the development of SST extremes. Indeed, they can be caused by a combination of atmospheric forcing and oceanic conditions/regimes, and can thus reveal different signals/processes also depending on the spatial scale considered (Holbrook et al., 2019). For instance, higher intensity MHWs are generally found in major western boundary currents, and in the eastern equatorial Pacific, where El Niño-Southern Oscillation (ENSO) events occur. In regions influenced by ENSO, events can persist for up to 2 months (Diaz & Markgraf, 2000; Holbrook et al., 2019). However, areas displaying greater frequencies and shorter duration events of abnormal warmer SST (and, in some cases, with higher intensities), may also be identified as MHW, though likely reflecting local variability in associated frontal position and related instabilities (e.g., see Figure 1 in Holbrook et al. (2019)). Upwelling regions, such as the Agulhas current, can be associated with MCS events, which like MHWs can have devastating effects on marine ecosystems (Lubitz et al., 2024). However, a detailed analysis of the drivers of MHWs is beyond the scope of the present work; a useful model-based discussion can be found in the recent study by Bian et al. (2024).

In this work we use gap-filled satellite-based SST products to investigate the sensitivity of MHW and MCS detection to algorithmic choices, illustrating the sensitivity to the key parameters such as the baseline period, the minimum duration and the threshold adopted, in a controlled setup and without ad-hoc choices, unlike, for example, Chiswell (2022). Additionally, the analysis is performed by decomposing the SST signal into low- and high-frequency components to respectively account for long-term changes and climate variability on the resulting extreme metrics, which are often used for both research studies and applications. This work is organized as follows: Section 2 provides information on the data used and methodological aspects, in Section 3 we present the results of our analysis, and Section 4 provides conclusions and perspectives for future work.

2. Methods and Data

2.1. Satellite SST Data

Accurate satellite observations have been providing continuous global mapping of SST for over four decades (Minnett et al., 2019), allowing for its exploitation in climate studies and applications. The main SST satellite data record used in this work is provided by the European Space Agency (ESA) Climate Change Initiative (CCI) and

the Copernicus Climate Change Service (C3S) (Merchant et al., 2019). This data set (version 2.1) provides daily global gap-free maps of SST at 20 cm nominal depth on a 0.05° × 0.05° regular grid, for the period from September 1981 to December 2022, based on thermal infrared measurements by the polar-orbiting Advanced Very High Resolution Radiometers, Along-Track Scanning Radiometers, and the Sea and Land Surface Temperature Radiometer. This data set has been produced by running the Operational Sea Surface Temperature and Sea Ice Analysis (OSTIA) system (Good et al., 2020). Performances of the data set have been evaluated for the period 1991–2012 as follows: its accuracy has been quantified in terms of bias of −0.04 K, computed as the global median difference of satellite minus drifting buoy SST; standard deviation of 0.34 K, computed as the robust standard deviation of differences of satellite and drifting buoy data; stability between −1.51 and −0.05 mK/year, computed at the 95% confidence interval for the relative multi-year trend between SSTs and the Global Tropical Moored Buoy Array. Some anomalous features have been evidenced, such as the apparently erroneous SSTs in 1982/3 likely due to the concomitance with the El Chichon eruption and the 1982/83 El Niño event, as evidenced in the SST CCI Climate Assessment Report (ESA, 2019).

Given its wide use in the literature, we also consider the daily OISST (Optimally Interpolated SST) data set (Huang, Liu, et al., 2021), produced by the National Oceanographic and Atmospheric Agency (NOAA), which is based on a combination of AVHRR infrared measurements, ship and buoy data. Version 2.1 of this data set (hereafter, NOAA) is available on a 0.25° × 0.25° spatial grid, with improvements over previous versions attributed to a revised processing of input in situ observations. A cold bias over the global oceans similar to CCI v2.1, but reaching up to −0.08 K in the Indian Ocean, has been identified (Huang, Liu, et al., 2021). Selected analyses for this data set can be found in Supporting Information S1, with some basic comparison between the CCI and NOAA data set in Figure S1 of the Supporting Information S1.

2.2. Data Preparation

Data preprocessing prior to analysis includes sea-ice masking considering only grid points never contaminated by ice and then remapping SST to a 1°×1° longitude-latitude grid. This is useful both to improve computational efficiency and for consistency with other relevant global data sets, such as the OceanSODA for biogeochemistry (Gregor & Gruber, 2021), so as to facilitate further ocean health studies. It is worth noting that relevant global studies such as Chiswell (2022) and Peal et al. (2023), used different SST data sets, but both similarly down-sampled the input data. On the other hand, the spatial characterization of multiple data sets presented in Yang et al. (2021) revealed that variability significantly declines for scales smaller than 100 km, thus motivating the analysis of SST extremes on the chosen grid.

The singular spectrum analysis (SSA) is a quite classic technique for time series analysis which has been applied in various fields of the physical and biological sciences, especially for relatively short records (Ghil et al., 2002; Schoellhamer, 2001). This method is designed to extract information on the dynamical system that generates a given time series, by decomposing the series in interpretable components ranging from trends to oscillatory modes and noise. Mathematically, the analysis starts from embedding a time series $X = X(t)$ of length N in a vector space of dimension M. This means that we construct a sequence of $N' = N - M + 1$ vectors of dimension M as copies of portions of X each shifted by one. The sequence of this so-called augmented vectors (Ghil et al., 2002) is used to construct the $N' \times M$ trajectory matrix D (Broomhead & King, 1986) composed by N' rows containing the augmented vectors and then to calculate the covariance matrix $C = \frac{1}{N'} D^T D$. The choice of size M depends on the competing requirements to best resolve the spectral dependence of the various components while preserving a sufficient number of repetitions of the oscillatory modes of eventual interest. That is, having a value of M as large as possible while keeping the number of repetitions of the M/N cycles reasonable, and also considering avoiding a covariance matrix C too large to diagonalize. As also suggested by Ghil et al. (2002) we use $M = N/10$ (i.e., 4 years) as a compromise between these competing needs.

Through the SSA, a time series can be reconstructed by only using a subset of k principal components A_k, obtained by projecting the original time series into each EOF. Dominant frequencies (determined by spectral analysis) can be associated with each eigenvector, therefore it is possible to limit the reconstruction to a chosen frequency interval (which depends on the choice of M). When the gravest principal component is removed, this is equivalent to a nonlinear detrending, with periodic and quasi-periodic oscillations, such as ENSO, and seasonal and higher frequency signals retained. Compared to other methods, the advantages of the SSA are its non-parametric nature, best suited to represent trends which may vary over time, and the avoidance of spectral distortion, common with

filtering approaches (Feliks et al., 2013). We label the resulting detrended time series SSA1, since only one mode is subtracted; alternatively, we subtract multiple eigenmodes with period below 1 year, that is, from the seasonal cycle to trends, and the corresponding time series is named SSAM. For comparison with previous works, we also include a linear detrending approach (LIN) which helps us understanding the effects of assuming a simple functional shape in the preprocessing step. Hereafter, we generically refer to these procedures as detrending.

2.3. Extremes Detection Algorithm and Validation

The starting point is the use of the standard Hobday's detection algorithm, that is,: 1991–2020 period to calculate the baseline climatology (following the WMO), the lower/upper deciles for thresholds (for MCSs and MHWs, respectively), 5 days for the minimum duration, and 2 days for the maximum gap between events, meant to reduce effects due to noise (e.g., spikes). Then, sensitivity to these parameters is explored in detail in Section 3, where we consider four locations of interest, namely grid points corresponding to the Gulf of Lyon (6°E–42°N), the equatorial Pacific (150°W–0°), the North Pacific (145°W–47°N), and the Tasman Sea (151°E–42°S). These locations are chosen since they have witnessed frequent MHWs in the last decades (A. Hobday et al., 2018; E. C. J. Oliver et al., 2018), and they are affected by long-term warming and substantial climate variability, for example due to ENSO. These regions are also mentioned in Capotondi et al. (2024) among the most MHW-affected regions not just in the historical record, but also in the last years. Wider regions, illustrated in Figure S2 of the Supporting Information S1, are used to increase the sample size to characterize the statistics of extremes in these hotspots. A MHW/MCS category is defined as the number of times a SST anomaly exceeds the difference between the percentile-based threshold and the climatology, and category 0 means no event (i.e., SSTs not exceeding the threshold). Following A. J. Hobday et al. (2016) and Gruber et al. (2021) here we consider a number of metrics useful to characterize the properties of extreme events, such as the cumulative intensity (the integral of the daily anomalies over the duration of an event), the maximum (for MHWs) or minimum (for MCSs) anomaly, the recurrence (calculated as the number of days between the end of an event and the onset of the next) and event duration.

We also compare the MHW results with the data set produced by NOAA under the Coral Reef Watch (v1.0.1) project (CRW hereafter). This data set provides MHW categories data from 1985 to present computed with a Hobday-like methodology (with a 1985–2012 baseline), using the CoralTemp SST (Maturi et al., 2017), which is based upon polar-orbiting and geostationary infrared imagery. Although not specified in their documentation, we have verified that events shorter than 5 days (according to Hobday's default approach) in the CRW data set are not filtered out (not shown). To match the spatial resolution of our CCI-based data sets, the data are remapped by taking the categorical mode for each 1° ×1° pixel, thus allowing direct comparison.

3. Results and Discussion

3.1. Low-Frequency Variability and Detection of Extremes

The occurrence of MHWs and MCSs is tied to variability at different spatial and temporal scales (Sen Gupta et al., 2020), and one major source influencing their occurrence is the long-term change due to global warming, illustrated in Figure 1. Most of the globe is characterized by a warming trend, which is stronger at mid-latitudes (up to 0.5 K/decade), such as in the North and South Pacific. Limited areas with neutral or negative trends are found in the equatorial Pacific Ocean (likely due a long-term increase in persistent La Niña events, X. Li et al. (2023)), in the Southern Ocean (Y. Dong et al., 2023) and in the North Atlantic (associated with the North Atlantic warming hole, Keil et al. (2020)).

To separate the contributions of long-term changes and short-term climate variability, we apply an SSA-based method to remove low-frequency variability. To illustrate the effects of this procedure, SST time series and Fourier spectra for pixels in the equatorial Pacific and the Tasman Sea are shown in Figures 2a and 2c–2f and in Figures 2b and 2g–2j, respectively. The variability in the two locations is very different: in the former, ENSO is the dominant signal, with well-defined warm anomalies exceeding 3 K followed by weaker and lingering cold anomalies; in the latter, variability has faster timescale and the magnitude of the anomalies is smaller (less than 2 K). The effects of preprocessing are different in the two areas, since in the equatorial Pacific linearly detrended and RAW SSTs overlap, and the SSA1 reduces the amplitude of the peaks, whereas in the Tasman Sea the SSA1 is more efficient than the LIN approach to remove long-term trends. In both cases, SSAM-based anomalies match the other time series especially when they change sign, likely since weather-related processes are leading such

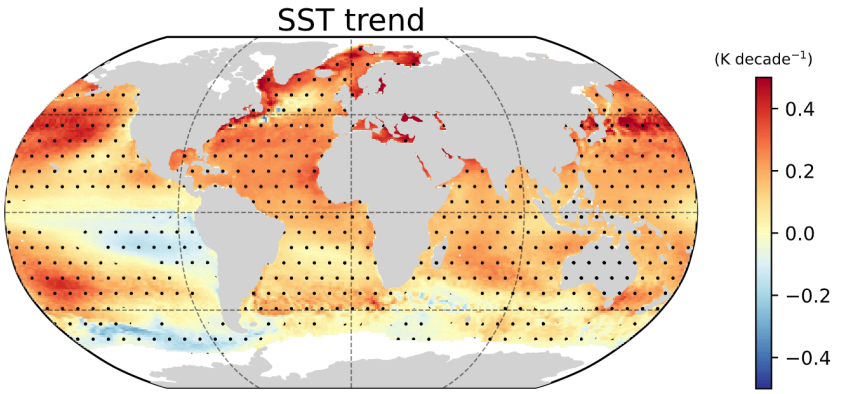

Figure 1. Linear trend of sea surface temperatures for the period 1982–2022, in K per decade. Regions with sea ice are masked, and significant trends ($p < 0.05$) are dotted.

periods. In terms of spectral analysis, for the Pacific Ocean, in the RAW data set (c), peaks are visible with periods between 3 and 7 years in the RAW and LIN data sets (Figures 2c and 2d), whereas for SSA1 (e) the variability with periods longer than 10 years is reduced, and the rest of the spectrum is unaffected. Although no significant variability is removed for LIN and SSA1 in the Tasman Sea, with SSAM (Figures 2f and 2j) all the spectral power with periods larger than 1 year is obliterated, leaving the signal corresponding to intraseasonal and faster modes of variability in the SST field only.

3.2. Sensitivity to Parameters Choice

The MHW/MCS detection algorithm depends on a number of numerical parameters, and here we show how results are affected by their settings for selected grid points. In this section we focus on CCI SST, as results for the NOAA data set are qualitatively similar. Although the long-term linear SST trend (Figure 1) certainly has an impact on the occurrence of extremes, in some regions low-frequency variability or long-term changes can be strongly nonlinear. We test the sensitivity of MHW detection to five different baselines periods: 1983–2012, 1985–2012 (A. J. Hobday et al., 2016), 1991–2020 as suggested by WMO, 1993–2021, often used in altimetry based studies, as well as the full period (1982–2022) (Figures 3a–3d). The number of extreme days is computed for events of any category above 0. For the RAW data set a clear dependence on the area chosen is observed, since results for earlier (e.g., 1985–2012) baseline periods differ from the most recent ones (with reductions up to 50%) except for the equatorial Pacific area. This can be explained by the different warming trends in that area (Figure 1), which, unlike other locations, are near zero or slightly negative. At all locations but the equatorial Pacific, for the RAW case using the full period for the climatology increases the detection rate compared to the WMO or altimetry baselines, almost doubling it in the North Pacific. For detrended data sets, as expected, results are nearly stationary across the different baselines, with variations of a few percent at maximum, and the agreement with the RAW data set is larger for the WMO baseline. Some nonlinearity is seen for the equatorial Pacific, with the 1993–2021 being the baseline with more events overall. It is worth noting that the SSA1 approach is more effective than LIN at removing the dependence on the baseline, as also discussed based on Figure 2b.

The threshold to identify a MHW is generally chosen as a tradeoff between the rarity of the events identified and the adequacy of the resulting sample size for applications. Most studies use the 90th percentile of the distribution at each point, meaning that roughly ten out of one hundred days would be identified as extreme. Actually, the number will be smaller since further algorithm steps (such as checking on the minimum duration) filter some of the events detected. Figures 3e–3h shows that the detection rate varies almost linearly (from 20% for the 80th to 1% for the 99th) with the chosen percentile at all locations, and this applies to both RAW and detrended SST time series. Among these locations, detection rates are larger even for the lower percentiles in the equatorial Pacific, likely due to the fact that MHWs are modulated by slowly evolving processes in that area, therefore they are not removed by checks applied on the minimum duration of the events.

Finally an important parameter we test is the minimum duration of the events (Figures 3i–3l). As it is common practice, we disregard events shorter than 5 days, since they are expected to have a reduced impact on marine

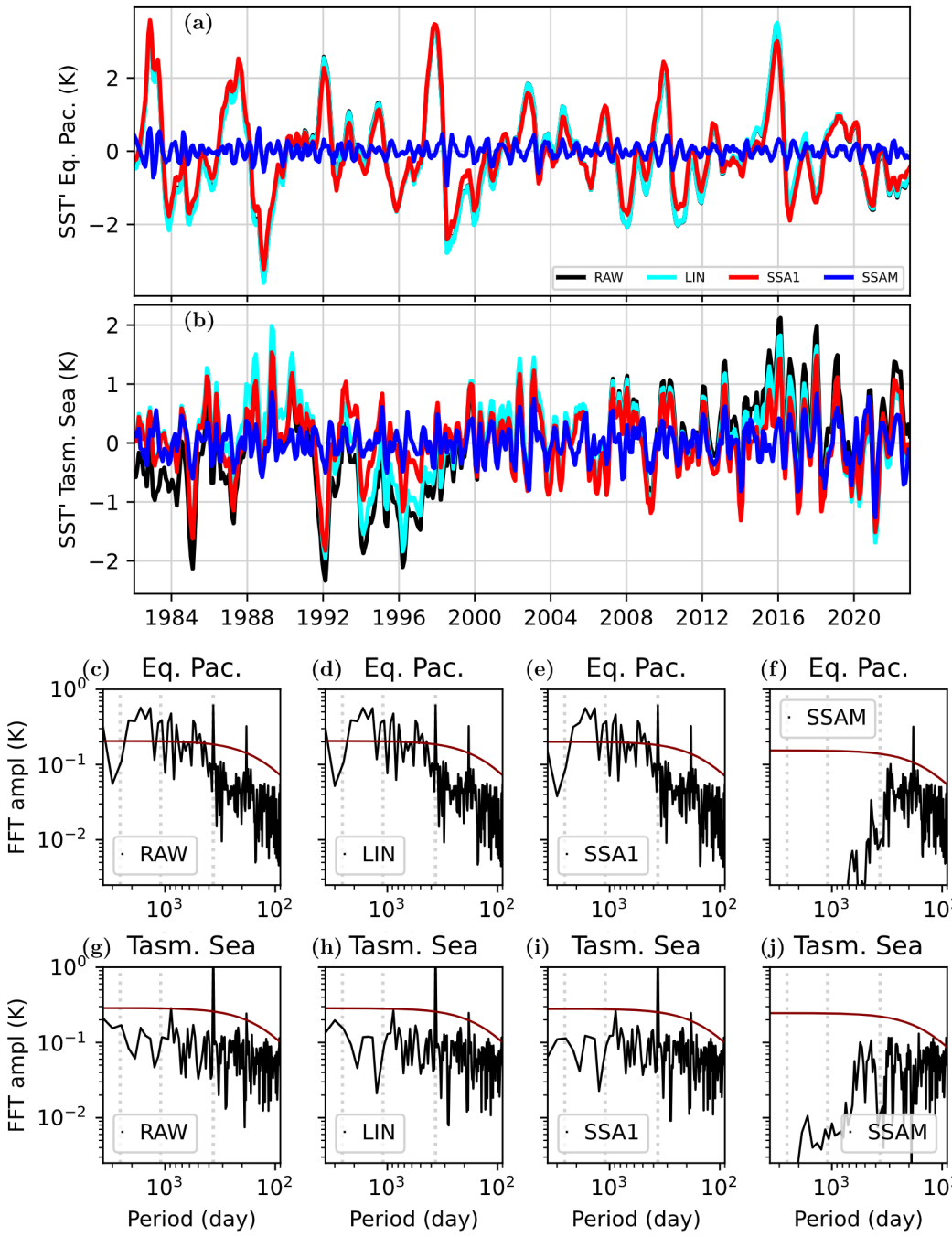

Figure 2. Monthly mean SST anomalies in the Niño 3.4 (a) and Tasman Sea (b), and Fourier spectra for the corresponding daily time series (c–f, g–j), following different preprocessing. In (c–j), peaks above the red line are significant compared to red noise at the 0.95 confidence level and thin vertical lines indicate 7, 3, and 1 years (from left to right).

ecosystems (Kauppi & Villnäs, 2022). We find that the detection rate strongly depends on the minimum duration parameter, with a faster drop between 5 and 15 days, and falling below 2% when the minimum duration is 25 days. Interestingly, the reduction is more gentle for the RAW and SSA1 data set in the equatorial Pacific (Figure 3i) compared for example, to the Tasman Sea (Figure 3l) again due to the timescales of the underlying ENSO forcings (also compare Figure 2a), whereas results are similar to other cases for the SSAM preprocessing. The results for LIN are generally close or somewhat higher than the RAW case across the regions considered, especially for shorter events.

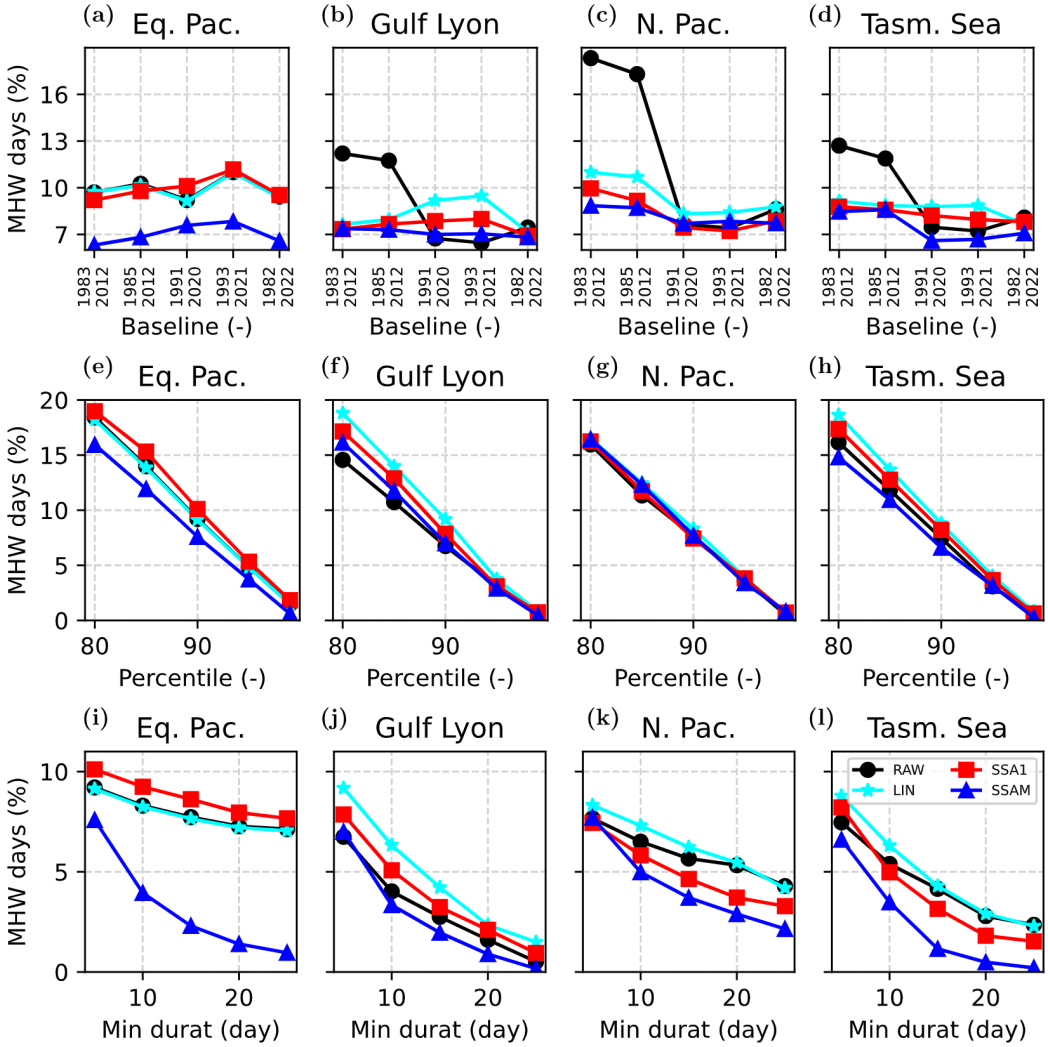

Figure 3. MHW detection sensitivity for the CCI data set to selected detection parameters: (a–d) the climatological baseline, (e–h) the percentile threshold, and (i–l) the minimum event duration.

A similar analysis for cold spells is presented in Figure 4, and results for percentile threshold and minimum duration are consistent with those found for MHWs. Interestingly, the number of MCS events detected is higher for the RAW data set, which may depend on asymmetries of the underlying SST distribution. Since less MCSs are expected owing to global warming, Figures 4a–4d clearly shows how choosing a later baseline (e.g., 1991–2020) generally increases the number of detected events. In fact, in the absence of other sources of low-frequency variability, a warmer climatology would favor the detection of cold extremes in the early portion of the record. In regions with strong trends (e.g., b–c), the difference goes from 50% to 100%. In turn, in areas affected by ENSO (Figure 4a) detrending (both LIN and SSA1) does not lead to a reduction of events for such later baselines, since trend is not dominant in those regions (Figure 1).

3.3. Characteristics of Extreme Events

A globally averaged and annually aggregated analysis of MHW/MCS categories can be used to understand long-term changes in extremes and their change upon detrending. In Figure 5, we show the temporal evolution of extreme events by considering the fraction of the ocean covered by an extreme of a certain category. A summary of the linear trends (% per decade) for MHWs and MCSs for the various detrending applied is given in Table 1. For MHWs, moderate and strong events appear to be increasing in recent years, whereas MCSs are decreasing

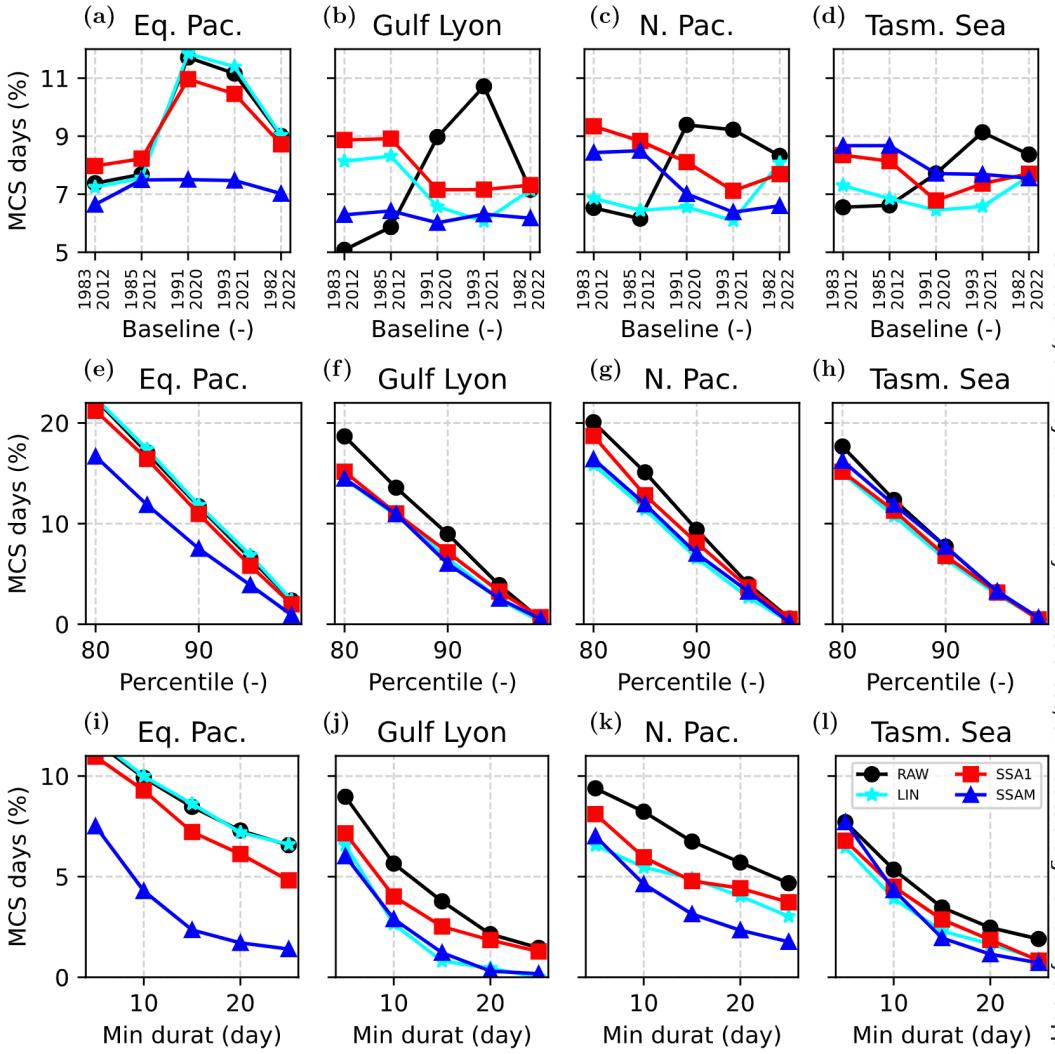

Figure 4. Same as the previous figure, but for MCS events in the CCI data set. Note that in (e–h) the percentile used for detection is 100 minus the value on the abscissa.

across all categories, with category 2 showing more marked changes. The magnitude of the trends in the non-event category (category 0) is similar for the two kinds of extremes. Likely due to the small sample size, trends in most severe events are insignificant. In agreement with Peal et al. (2023), there is a long term increase in MHW and a reduction of MCS events with time when the trend is not removed. Interestingly, they have found that MCS of Cat 3 and 4 have remained constant with time, whereas in our case there is a reduction of Cat 3 and only Cat 4 events show no significant trend, and we do not find the increase of extreme events discussed by Peal et al. (2023) either. We note that a source of discrepancy with previous works is that we exclude grid points with sea ice coverage, which could introduce spurious drifts in areas becoming ice free for a longer part of the year, such as the Southern and the polar oceans.

For both MHWs and MCSs, the effects of detrending are clearly visible for the SSA1 and SSAM cases, as for example, the trends in the ocean experiencing no events (Cat 0) virtually disappear after detrending. Decadal changes in individual categories are more complex and generally insignificant, but for MHWs the removal of long-term trends done for SSA1 tends to promote the occurrence of moderate events at the expense of stronger ones. Conversely, for MCSs, the extreme category is more likely after detrending, which suggests different mechanisms driving these two extremes, as also discussed by Wang et al. (2022).

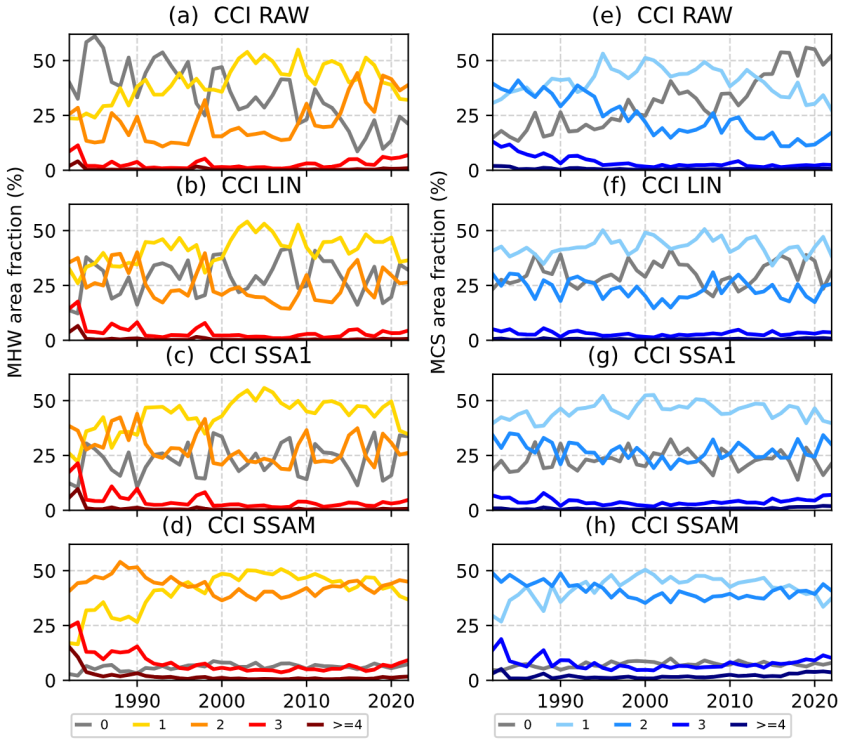

Figure 5. Time series of the fraction of the sea where the annual heatwave (left column) and cold spell (right column) extremum is category 0 (no event detected, gray), 1 (moderate), 2 (strong), 3 (severe) or equal or beyond 4 (extreme) for the (a–e) RAW, (b–f) LIN, (c–g) SSA1, and (d–h) SSAM data sets.

It is informative to compare the results obtained for CCI with those based on the NOAA SSTs, reported in Figure S3 of the Supporting Information S1. For the RAW case, the trend in Cat 0 is more marked for both MHWs and MCSs. Although the results for the LIN and SSA1 detrending methods are in good agreement with the CCI case, the trends in Cat 1 and Cat 2 in SSAM remain apparent throughout the time series. This would suggest that while the representation of large-scale drivers in the CCI and NOAA data sets is consistent, there may be discrepancies for smaller scale events. Differences may depend on a variety of factors, such as the input data considered, or how atmospheric correction is performed.

Table 1
Global Linear Trends (as Change in 1°×1° Pixels, in % Area Per Decade) for Warm and Cold Marine Extremes by Category, for All Preprocessing Cases

Event/Processing	Cat 0	Cat 1	Cat 2	Cat 3	Cat 4+
MHW/RAW	**−8.74**	**4.09**	**4.66**	0.12	−0.13
MHW/LIN	0.88	**2.49**	−1.75	**−1.25**	**−0.37**
MHW/SSA1	1.27	**3.18**	**−2.11**	**−1.76**	**−0.58**
MHW/SSAM	**0.49**	**4.62**	**−1.29**	**−2.67**	**−1.15**
MCS/RAW	**9.57**	−0.49	**−7.05**	**−1.86**	**−0.16**
MCS/LIN	0.75	0.33	**−1.04**	−0.12	0.08
MCS/SSA1	0.08	0.50	−0.84	0.04	**0.22**
MCS/SSAM	**0.46**	1.40	**−1.72**	−0.46	0.32

Note. Bolded values indicate significant trends ($p < 0.05$).

Spatially resolved analysis of the MHW/MCS metrics and their changes has been reported previously (Chiswell, 2022; Peal et al., 2023), and here we discuss how results change when applying different detrending methods. Figure 6 shows spatial maps of MHW average cumulative intensity, which is one of the most relevant metrics for impacts (Garrabou et al., 2022; Smith et al., 2023), as it combines duration and intensity. The tropical Pacific is the major hotspot of MHW events (Figures 6a–6c), followed by the regions with strong frontal activity, such as the Gulf Stream or Kuroshio currents, as already shown by Chiswell (2022), which remains also after the SSAM preprocessing (Figure 6d). The departures of LIN and SSA1 from RAW are spatially similar, but SSA1 more effectively suppresses the MHW signal in the southern hemisphere, whereas SSAM is more negative everywhere except for coastal regions in the northern hemisphere (Figures 6e–6g). As expected from Figure 1, the nonlinear detrending (SSA1) removes much of the long-term changes in MHW intensity Figures 6e–6g, whereas trends are further reduced globally for the SSAM case. For MHWs, we find that pixel-level noise is still apparent at the 1° resolution used here, and that spatial coherence is increased with the SSA1 approach compared to LIN. MCSs frequently appear along Western Boundary Currents regions (Figures 7a–7d), and this is

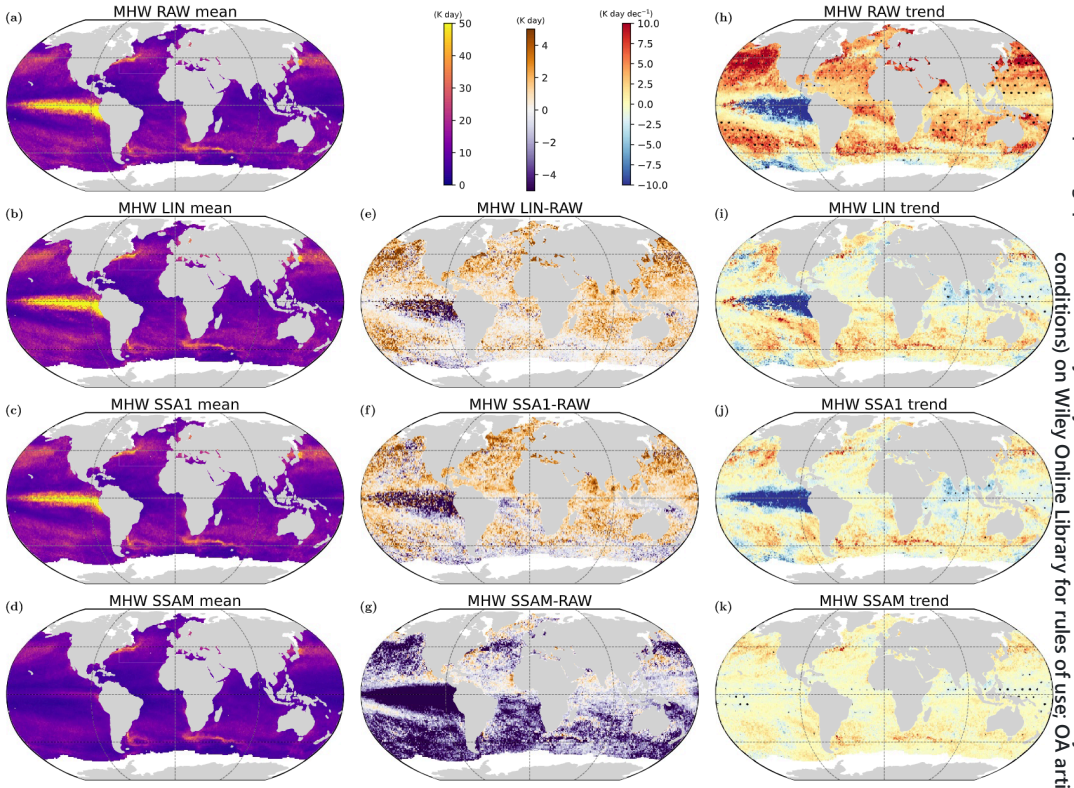

Figure 6. Spatial maps of average cumulative intensity of MHWs (expressed in K day, a–d), corresponding differences between detrended and RAW data sets (e–g), and linear trends (in K day/decade, plots h–k, with areas above the 95% confidence level dotted).

little affected by the detrending applied. Turning our attention on MCSs, the effect of detrending is not only to reduce their cumulated intensity but also to increase it in regions such as the Southern Ocean and southern Atlantic (Figures 7e–7g). The RAW global trend (Figure 7h) is dominantly positive, with an overall reduction of the cumulative intensity (which is negative, by definition) except for more severe events occurring in the tropical Pacific, Southern Ocean and in the Gulf Stream region. Both LIN and SSA1 lead to a negative trend in the latter regions, frequently accompanied by a compensating response in surrounding areas, such as in the southern Atlantic and Pacific.

To compare with previous works, the same analysis is repeated for the NOAA SSTs, reported in Figures S4 and S5 of the Supporting Information S1. Despite a good agreement on the large scale patterns, the detailed structure of the trends is different; with MHWs exhibiting a less intense negative trend in the tropical Pacific and Indian Oceans and a stronger trend in the Atlantic. The main differences in MCS trends between the two data sets are found across the Pacific, at all latitudes. It is worth noting that the departures of the LIN and SSA1 detrending from RAW are less marked compared to CCI in the Southern Ocean and more prominent in the North Pacific, as seen in maps e–f.

Given long-term changes and the effects of detrending, an important metric to monitor is the recurrence of the events. In this case, we compare the average for MHWs and MCSs over the period 1982–2022 (Figure 8), which shows how SSA-based detrending (c–d and g–h) tends to reduce the interval between events, likely because weaker but more frequent events are promoted. This effect is mostly visible for the SSAM case for both MHWs and MCSs, for which the recurrence is more than halved in the tropics, where ENSO is a dominant mode of variability. Interestingly, this does not appear to be the case globally for the LIN detrending, as recurrence times are actually increased in the tropical Pacific and Northern Atlantic (h). Discrepancies in this metric between MHW and MCS suggest that their sensitivity to a warming baseline is different (Peal et al., 2023).

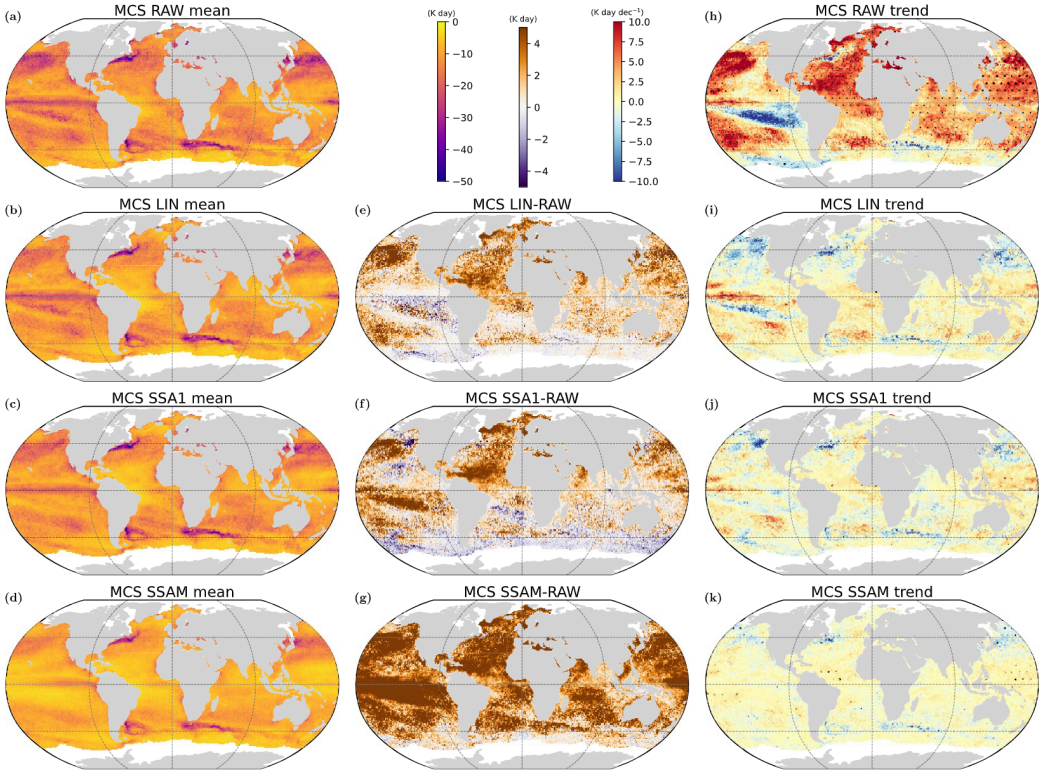

Figure 7. As in the previous figure, but for MCSs.

To further quantify the effects of detrending, we present in Figures 9 and 10 the distribution of the main MHW/MCS metrics, across selected hotspot regions (Figure S2 in Supporting Information S1). Most distributions (except that for the maximum intensity, plots e–h) are heavy-tailed, with a shape depending on the selected area. The largest tails, especially for intensity metrics, are found in the equatorial Pacific area, more markedly for MHWs, due to the modulation of ENSO (Figure 9), as peaks are only marginally affected by detrending (Figure 2a). Compared to RAW, intensity metrics are reduced on average by 10% for the LIN case, and by 20% for the SSA1 case in all regions except for the equatorial Pacific. Comparing Figures 9 and 10, markedly different responses to detrending between MHW and MCS events can be noted for the Gulf of Lyon region, as detrending has little impact for MHWs, whereas for LIN and SSA1 MCS duration is progressively reduced. The recurrence period, as already found in the previous section, is actually longer (more than doubled for the Gulf of Lyon and North Pacific) after the LIN preprocessing for MCS (Figures 10m–10p), whereas it is similarly reduced for MHWs (Figures 9m–9p). The impact of SSAM is qualitatively the same of SSA1, but much more pronounced, distributions tend to be close to each other after such aggressive preprocessing. This indicates that common driving processes remain when retaining only intra-annual timescales.

To validate our MHW detection with the CCI data set, we now provide a comparison with the independent CRW product. Time series of the area of the ocean affected by MHWs is reported in Figure 11a. Results for the CRW and the CCI data set with the same baseline (1985–2012) are in good agreement, but there is a small systematic offset which may be due to the different underlying SST data sets and the inclusion of short events in the CRW product. The major source of interannual variability in the CRW and non-detrended CCI data sets is represented by El Niño events (peaks around 1983, 1997, 2010, and 2016). However, these data set. also show heightened occurrences of MHWs in the last decade, despite the triple-dip La Niña in 2020–2022 (X. Li et al., 2023), which are due to long-term warming trends. Although the CRW data set is unavailable for the early portion of the record, all CCI data sets display overall maxima of occurrence (almost 30% of the global ocean under MHWs for RAW, more for the detrended data sets) in that period, when a major El Niño occurred (Caviedes, 2001). Nevertheless, these values, which are also present in the analysis of Peal et al. (2023), may be due to SST artifacts present in the early record, and they do not appear in the corresponding NOAA time series (Figure S6a in Supporting

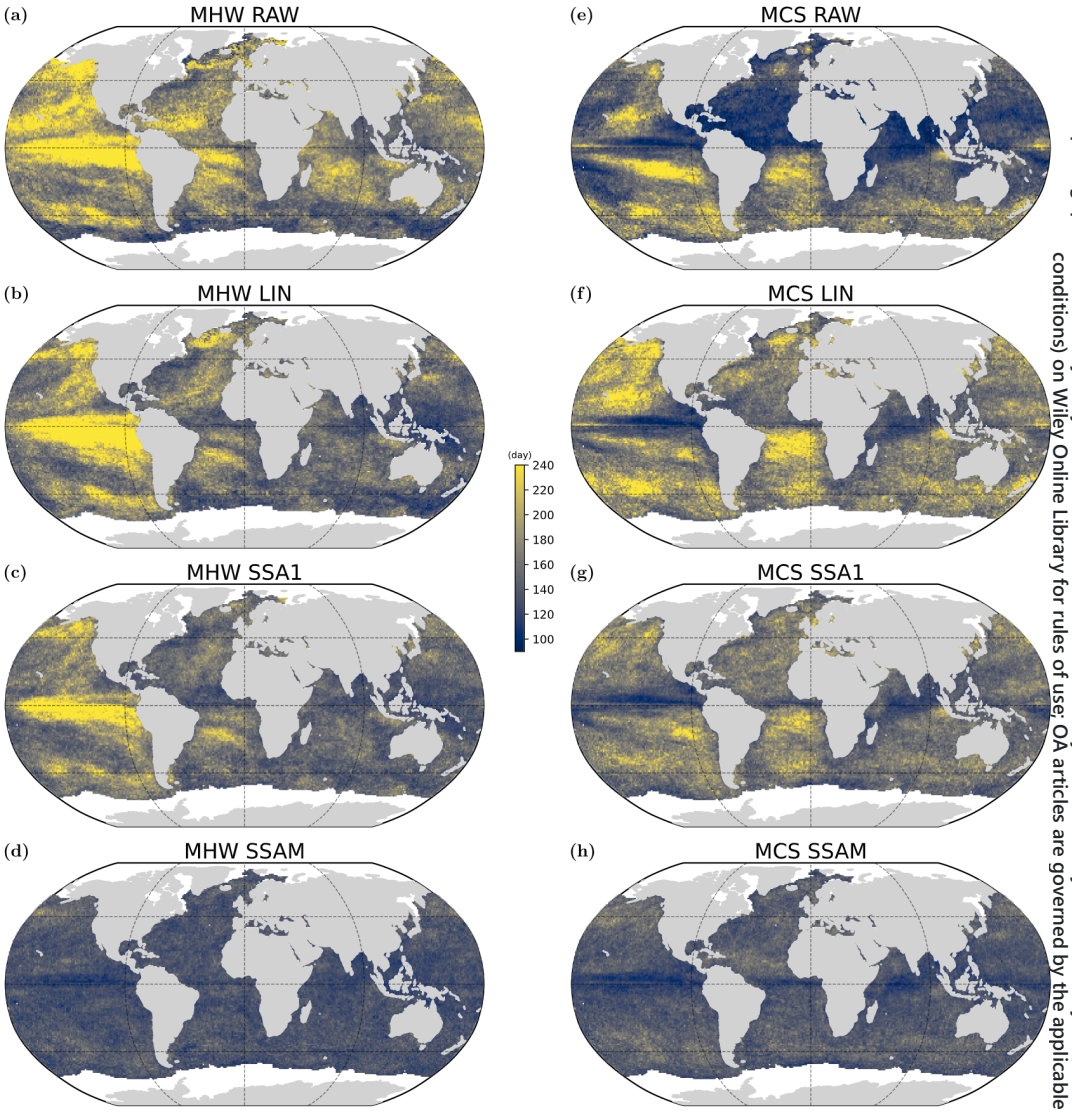

Figure 8. Average recurrence for MHWs (a–d) and MCSs (e–h).

Information S1). In particular, around the 1982/83 El Niño a strong anomaly (0.5 K) stands out in CCI tropical SSTs, differently from the NOAA data set (also refer to Figure S2 in Supporting Information S1). In fact, repeating the same analysis with NOAA SSTs, the peaks around this period are absent, indicating that the SSTs bias is reflected in the detected MHWs. The agreement between the two data sets improves after only 1990, but outstanding differences are visible around 2020 for the RAW case. As expected, the detrending removes long-term increase of MHW occurrence, and while the SSA1 and SSAM are generally aligned with the CRW and RAW data sets, they show additional local maxima in the late 1980s and early 1990s. As found in previous analyses, whereas there is qualitative agreement between the LIN and SSA1 cases, the latter seems more effective in reducing the MHW-affected area throughout the time series.

Figures 11b–11e report probability distributions of MHW categories for selected regions, also used for Figures 9 and 10. In general there is approximately a factor 10 decrease as MHW category is increased (e.g., category 2 events are 10 times less likely than category 1). Categories 3 and 4 are more frequent where SST warming trends are higher (Figure 1). The agreement between the CRW and the CCI data set with the same baseline is good, with some discrepancies for the higher categories: except for the Tasman Sea (Figure 11e), CRW tends to showcase less frequent category 4 events, whereas the CCI data set with baseline 1985–2012 has more category 3 events than others. These differences can be explained by the different SST data sets used between CRW and our work,

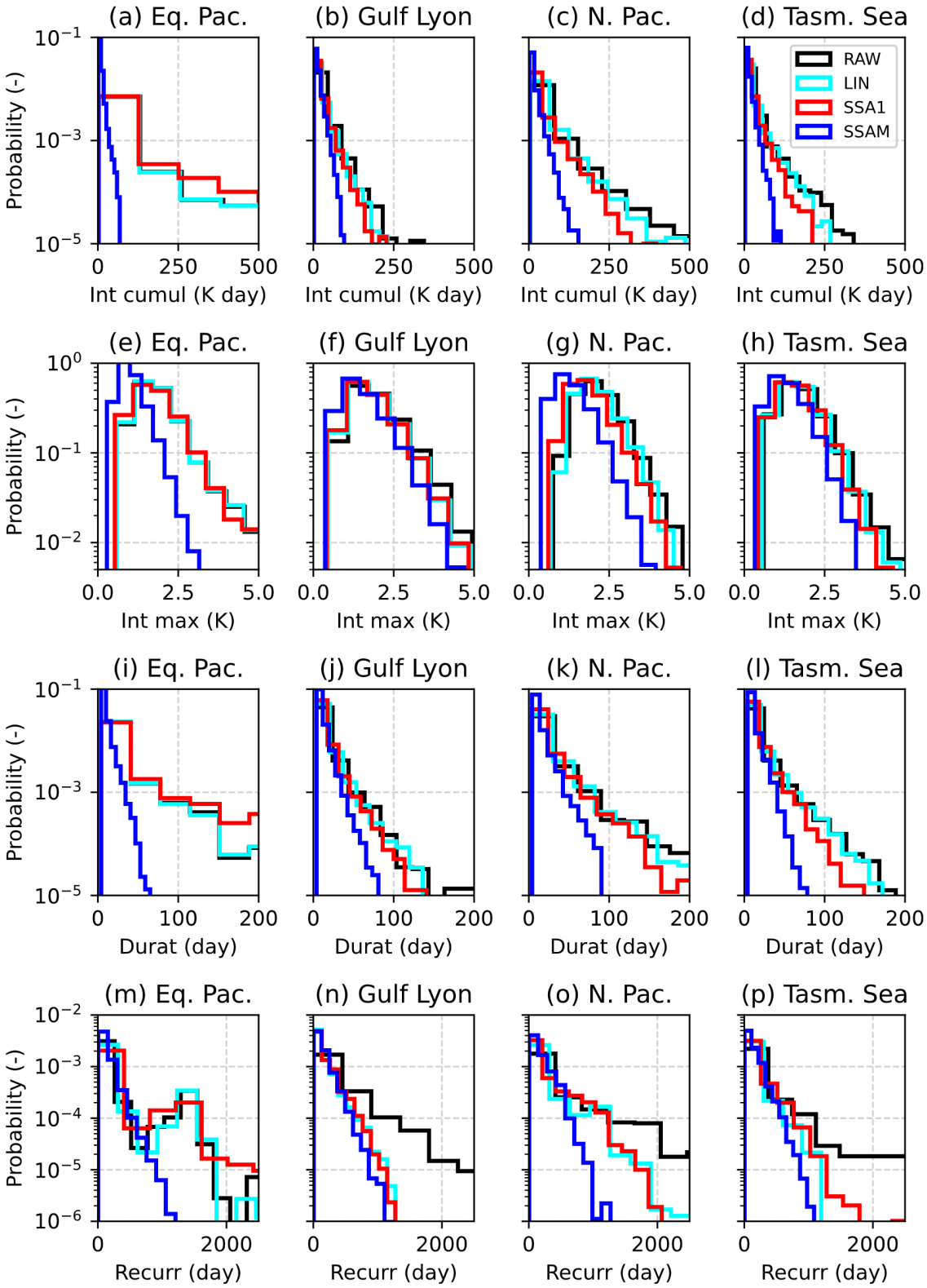

Figure 9. Histograms of MHW metrics (cumulative intensity, a–d, maximum intensity, e–h, duration, i–l, and recurrence, m–p) in the CCI data set, for selected regions and postprocessing methods.

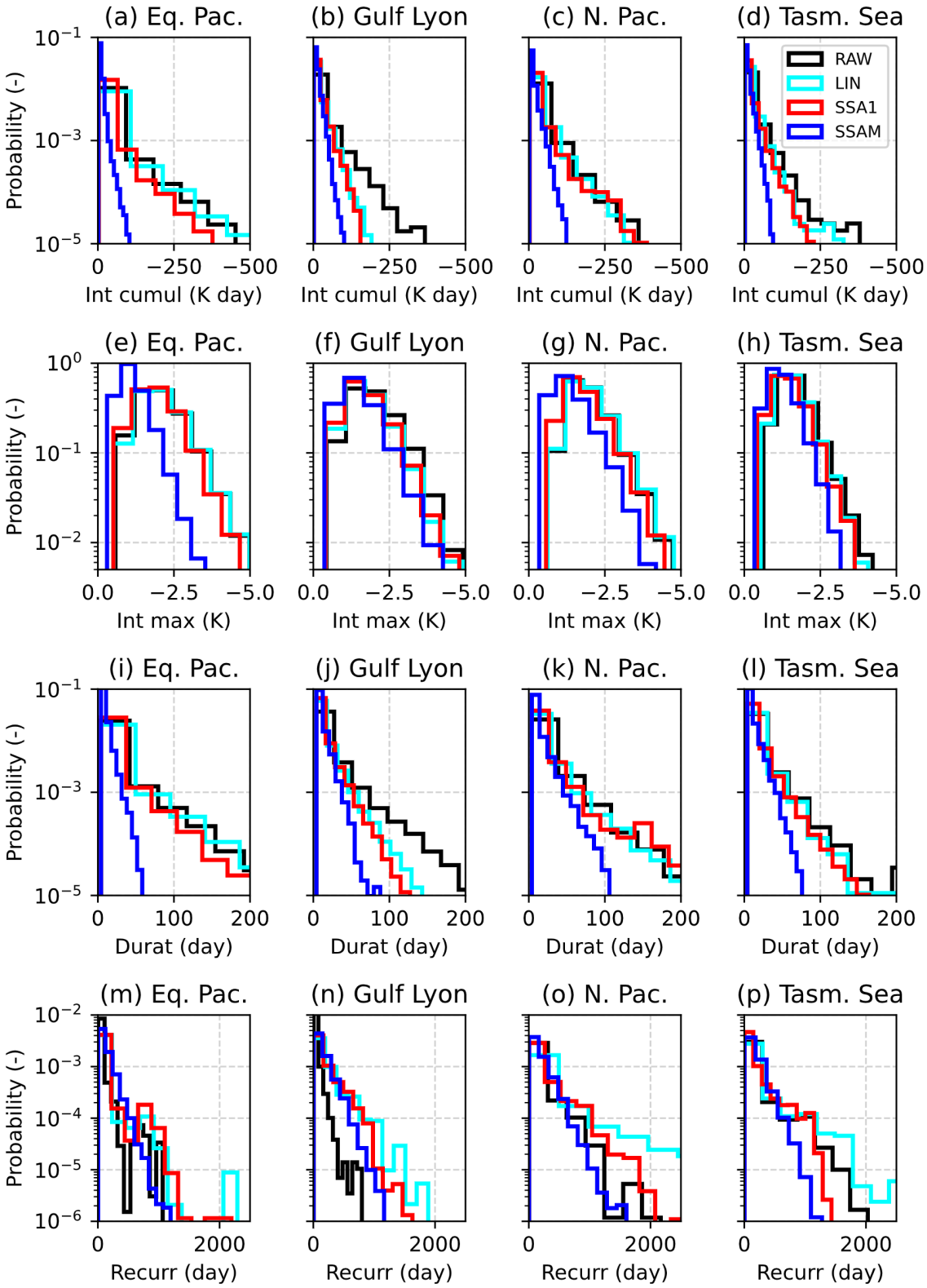

Figure 10. As in Figure 9, but for MCS in the CCI data set.

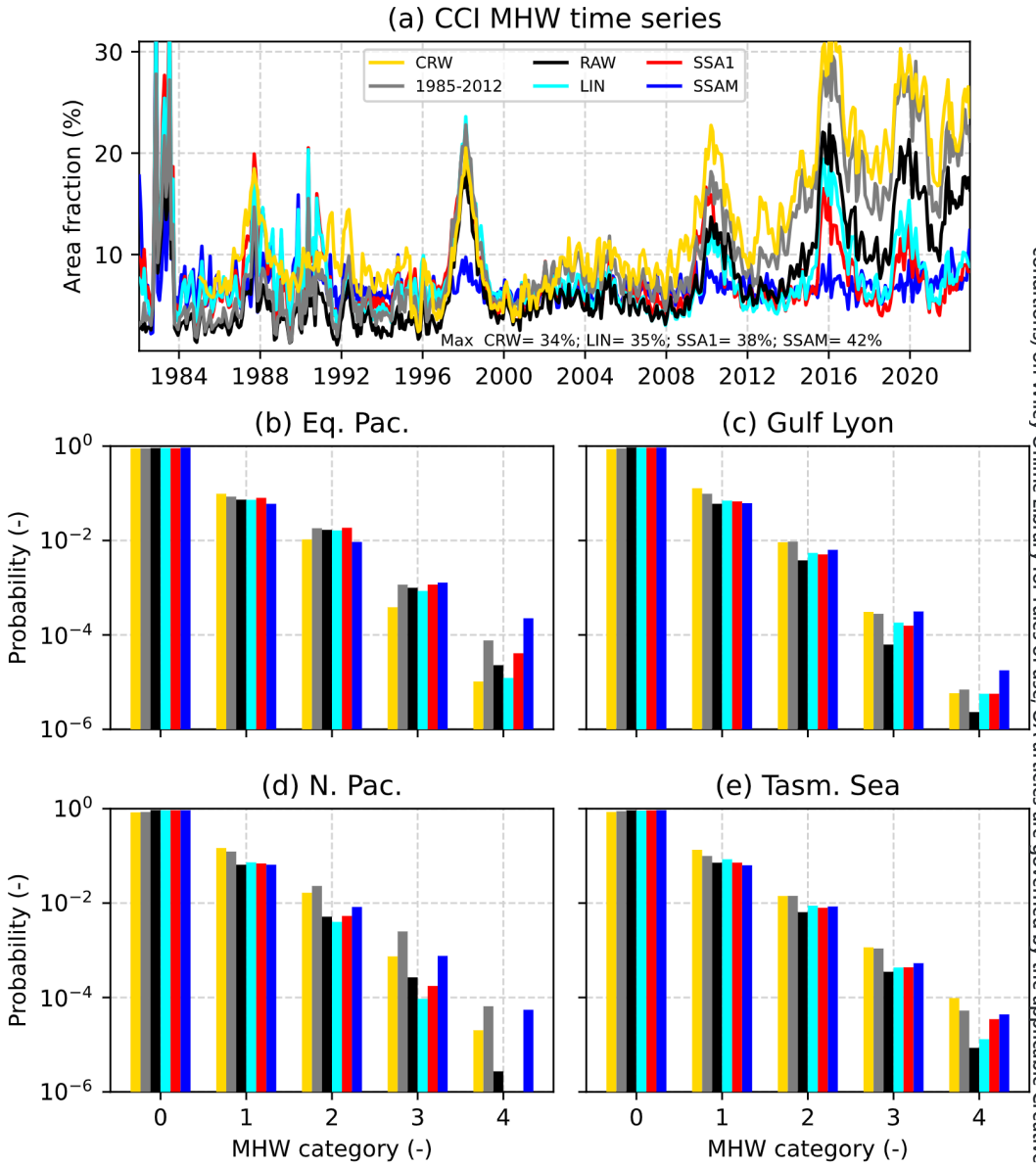

Figure 11. (a) Monthly mean time series of the fraction of the ocean with MHW category 1 or above for the various data sets (baselines 1985–2012 for gray and yellow lines, 1991–2020 otherwise). Maxima of time series overshooting the upper ordinate bound are reported with text. (b–e) Histograms of daily MHW categories for the different data sets, over the common period 1985–2022 and for selected regions (see Figure S2 in Supporting Information S1).

which could be important in areas frequently affected by cloud cover such as the tropics and high latitudes. A process-oriented and seasonally stratified analysis would be needed to better understand these discrepancies. Category 4 events are also present in SSA1 and SSAM, and are relatively frequent in the latter (Figures 11b and 11e) compared to the non-detrended data sets. This could be explained by the increased importance of shorter and noisy conditions after the removal of lower frequency and large-scale modulations. On the other hand, both LIN and SSA1 detrending methods systematically reduce the likelihood of MHW events across categories 1–3 compared to the RAW case (except for the equatorial Pacific area). Similar results hold for the histograms based on the NOAA SSTs (Figure S6 in Supporting Information S1).

4. Discussion and Conclusions

In this work we investigate the sensitivity of the detection of MHW and MCS in satellite-based SST data sets to algorithmic choices and quantify the impact of nonlinear detrending, which can be used to isolate the effects of global warming and more in general of low-frequency variability. The detection is based on the widely used algorithm proposed by A. J. Hobday et al. (2016), which provides a discrete categorization of warm and cold extremes, and a set of metrics to characterize individual events. The detection is performed in ice-free regions, since the treatment of SST below sea ice depends on the data sets and could introduce detection biases.

We find that the choice of the detection parameters is critical, and their values need to be set subjectively. In particular, the use of a fixed baseline (e.g., 1983–2012) has been advocated by A. Hobday et al. (2018) based on the availability of satellite-based SST records, even if there is no consensus on this choice (Sen Gupta, 2023), and for observation-based products relying on altimetry data (available after 1993) only more recent climatologies can be constructed. The choice of this parameter is critical, for example, for determining the MHW saturation effect found in climate simulations (Tanaka & Houtan, 2022). We show that a difference of 10 years in the baseline period leads to differences up to 50% in the number of SST extremes detected where strong trends are present, such as in the Mediterranean Sea and North Pacific. As expected, the effects for MCSs mirror those for MHWs in the same regions, given the global warming trend. Other relevant parameters we tested are the percentile threshold used to define events and their minimum duration, with the number of extremes detected decreasing linearly for the former (with little influence from detrending), and more variably for the latter, depending on the local timescale of MHW/MCS events. The decrease is steeper in regions where events are weather-driven and shorter.

We employ an SSA-based method to remove low-frequency changes and isolate events driven by weather conditions. This approach has the advantage of being data-driven, non-parametric and more suited to treat short and noisy time series. We demonstrate its effectiveness at removing the global warming influence over simple linear detrending, but also that there may be compensating effects, for example, with the promotion of more frequent and weaker, versus rare but stronger events (Figure 5). For this reason, MHW/MCS categories should preferably be considered together with physically interpretable metrics, such as intensity. Our analysis provides a possible way to determine if low-frequency variability, rather than fast weather forcing, has been the major factor determining the occurrence of a SST extreme, even if we cannot infer which the main driver is without considering other data. The global analysis revealed how detrending affects the detection of extremes, with the areas of the Brazilian Current, the Gulf Stream, the Kuroshio and the Antarctic Circumpolar in the Atlantic/Indian sector appear to be hotspots also after detrending. Extremes are detected in those regions due to stochastic fluctuations in the location of fronts, and a correct description of these events, likely mediated by eddy processes, would need high-resolution data sets (Hayashida et al., 2020; Kirtman et al., 2017; Pilo et al., 2019).

Although the trends in the raw SST data set for both MHW and MCS are consistent with the literature, we find that the effect of detrending is to reduce the probability of high intensity extremes and to favor weaker events, which also tend to occur more frequently. Some discrepancies with the literature may be due to different treatments of areas with sea ice, whose distribution departs from normality making the standard detection approach unsuitable (Huang, Wang, et al., 2021). We also note that results after SSA-based detrending appear to be spatially more coherent compared to the linear approach, which we attribute to their ability to capture quasi-periodic signals which often happen to be spatially correlated. A comparison with an independent MHW data set based on a different SST product shows a good agreement for the raw SST results, with some discrepancies in the early phase of the record, when data coverage was sparser and contamination due to volcanic eruptions are likely (leading to regional biases up to 0.5 K, Figure S1 in Supporting Information S1).

Our analysis indicates how the detection of MHWs and MCSs depends on the algorithmic setup, making comparisons between different works challenging. Whilst most parameters cannot be constrained from theoretical considerations, as a general recommendation we believe it is useful to be consistent with previous works and include comparisons with peer data sets, which are now increasingly available. Based on the current warming trajectory, non-parametric detrending should be preferred since the trend is increasingly nonlinear (Chiswell, 2022). Further research is needed to evaluate possible discrepancies in extremes detected across satellite-based SST products, as the input data set can be a source of uncertainty. This may arise from the treatment of cloudy pixels, sea ice covered areas, different input observations, and possible retrieval issues in the early satellite era, which could affect results when early baselines are adopted for detection.

Conflict of Interest

The authors declare no conflicts of interest relevant to this study.

Data Availability Statement

The CCI SST (v2.1) data set is publicly available from: https://cds.climate.copernicus.eu/cdsapp#!/dataset/satellite-sea-surface-temperature?tab=form (https://doi.org/10.24381/cds.cf608234), and the NOAA Coral Reef Watch MHW data set is available at https://coralreefwatch.noaa.gov/product/marine_heatwave/. The OISST V2 High Resolution Data set is provided by the NOAA PSL, from their website at https://psl.noaa.gov. The software for the event detection is online at https://github.com/ecjoliver/marineHeatWaves. The RAW and SSA1 MHW and MCS products based on CCI SST data are available from https://zenodo.org/records/8154587; the SSA4 data sets can be accessed from https://zenodo.org/records/13771592. All links were last accessed in April 2025.

Acknowledgments
We appreciate constructive suggestions from three anonymous reviewers. The authors received funding by the "CAREHeat–deteCtion and threAts of maRinE Heat waves" project, funded by the European Space Agency (Contract No. 4000137121/21/I-DT). VDT has also been supported by a Copernicus Climate Change Service project (C3S2_601). We are grateful to Eric Oliver for sharing the MHW/MCS detection code. Open access publishing facilitated by Consiglio Nazionale delle Ricerche, as part of the Wiley - CRUI-CARE agreement.

References

Anav, A., Antonelli, M., Calmanti, S., Carillo, A., Catalano, F., Dell'Aquila, A., et al. (2024). Dynamical downscaling of CMIP6 scenarios with ENEA-REG: An impact-oriented application for the Med-CORDEX region. *Climate Dynamics*, *62*(5), 3261–3287. https://doi.org/10.1007/s00382-023-07064-3

Bian, C., Jing, Z., Wang, H., & Wu, L. (2024). Scale-dependent drivers of marine heatwaves globally. *Geophysical Research Letters*, *51*(3), e2023GL107306. https://doi.org/10.1029/2023GL107306

Broomhead, D. S., & King, G. P. (1986). Extracting qualitative dynamics from experimental data. *Physica D: Nonlinear Phenomena*, *20*(2), 217–236. https://doi.org/10.1016/0167-2789(86)90031-X

Capotondi, A., Rodrigues, R. R., Sen Gupta, A., Benthuysen, J. A., Deser, C., Frölicher, T. L., et al. (2024). A global overview of marine heatwaves in a changing climate. *Communications Earth & Environment*, *5*(1), 1–17. https://doi.org/10.1038/s43247-024-01806-9

Caviedes, C. (2001). *El Niño in history: Storming through the ages*. University Press of Florida.

Chiswell, S. M. (2022). Global trends in marine heatwaves and cold spells: The impacts of fixed versus changing baselines. *Journal of Geophysical Research: Oceans*, *127*(10), e2022JC018757. https://doi.org/10.1029/2022JC018757

Ciappa, A. C. (2022). Effects of Marine Heatwaves (MHW) and Cold Spells (MCS) on the surface warming of the Mediterranean Sea from 1982 to 2018. *Progress in Oceanography*, *205*, 102828. https://doi.org/10.1016/j.pocean.2022.102828

Diaz, H. F., & Markgraf, V. (Eds.) (2000). *El Niño and the southern oscillation: Multiscale variability and global and regional impacts*. Cambridge University Press.

Dong, L., Zeng, S., Song, F., Wu, L., Shi, J., Ding, Y., & Lv, S. (2024). Roles of external forcing and internal variability in global marine heatwaves change during 1982–2021. *Geophysical Research Letters*, *51*(4), e2023GL107557. https://doi.org/10.1029/2023GL107557

Dong, Y., Polvani, L. M., & Bonan, D. B. (2023). Recent multi-decadal southern ocean surface cooling unlikely caused by southern annular mode trends. *Geophysical Research Letters*, *50*(23), e2023GL106142. https://doi.org/10.1029/2023gl106142

ESA. (2019). Climate Assessment Report (CAR) SST CCI-CAR-UKMO-201 (Technical Report). Retrieved from https://climate.esa.int/documents/268/SST_cci_CAR_v1.pdf

Feliks, Y., Groth, A., Robertson, A. W., & Ghil, M. (2013). Oscillatory climate modes in the Indian monsoon, North Atlantic, and tropical Pacific. *Journal of Climate*, *26*(23), 9528–9544. https://doi.org/10.1175/JCLI-D-13-00105.1

Frölicher, T. L., Fischer, E. M., & Gruber, N. (2018). Marine heatwaves under global warming. *Nature*, *560*(7718), 360–364. https://doi.org/10.1038/s41586-018-0383-9

Garrabou, J., Gómez-Gras, D., Medrano, A., Cerrano, C., Ponti, M., Schlegel, R., et al. (2022). Marine heatwaves drive recurrent mass mortalities in the Mediterranean Sea. *Global Change Biology*, *28*(19), 5708–5725. https://doi.org/10.1111/gcb.16301

Ghil, M., Allen, M. R., Dettinger, M. D., Ide, K., Kondrashov, D., Mann, M. E., et al. (2002). Advanced spectral methods for climatic time series. *Reviews of Geophysics*, *40*(1), 3-1–3-41. https://doi.org/10.1029/2000rg000092

Good, S., Fiedler, E., Mao, C., Martin, M. J., Maycock, A., Reid, R., et al. (2020). The current configuration of the OSTIA system for operational production of foundation sea surface temperature and ice concentration analyses. *Remote Sensing*, *12*(4), 720. https://doi.org/10.3390/rs12040720

Gregor, L., & Gruber, N. (2021). OceanSODA-ETHZ: A global gridded data set of the surface ocean carbonate system for seasonal to decadal studies of ocean acidification. *Earth System Science Data*, *13*(2), 777–808. https://doi.org/10.5194/essd-13-777-2021

Gruber, N., Boyd, P. W., Frölicher, T. L., & Vogt, M. (2021). Biogeochemical extremes and compound events in the ocean. *Nature*, *600*(7889), 395–407. https://doi.org/10.1038/s41586-021-03981-7

Hayashida, H., Matear, R. J., Strutton, P. G., & Zhang, X. (2020). Insights into projected changes in marine heatwaves from a high-resolution ocean circulation model. *Nature Communications*, *11*(1), 4352. https://doi.org/10.1038/s41467-020-18241-x

Hobday, A., Oliver, E., Sen Gupta, A., Benthuysen, J., Burrows, M., Donat, M., et al. (2018). Categorizing and naming marine heatwaves. *Oceanography*, *31*(2). https://doi.org/10.5670/oceanog.2018.205

Hobday, A. J., Alexander, L. V., Perkins, S. E., Smale, D. A., Straub, S. C., Oliver, E. C. J., et al. (2016). A hierarchical approach to defining marine heatwaves. *Progress in Oceanography*, *141*, 227–238. https://doi.org/10.1016/j.pocean.2015.12.014

Holbrook, N. J., Scannell, H. A., Sen Gupta, A., Benthuysen, J. A., Feng, M., Oliver, E. C. J., et al. (2019). A global assessment of marine heatwaves and their drivers. *Nature Communications*, *10*(1), 2624. https://doi.org/10.1038/s41467-019-10206-z

Huang, B., Liu, C., Banzon, V., Freeman, E., Graham, G., Hankins, B., et al. (2021). Improvements of the Daily Optimum Interpolation Sea Surface Temperature (DOISST) version 2.1. *Journal of Climate*, *34*(8), 2923–2939. https://doi.org/10.1175/JCLI-D-20-0166.1

Huang, B., Wang, Z., Yin, X., Arguez, A., Graham, G., Liu, C., et al. (2021). Prolonged marine heatwaves in the Arctic: 1982–2020. *Geophysical Research Letters*, *48*(24), e2021GL095590. https://doi.org/10.1029/2021gl095590

Kajtar, J. B., Holbrook, N. J., Lyth, A., Hobday, A. J., Mundy, C. N., & Ugalde, S. C. (2024). A stakeholder-guided marine heatwave hazard index for fisheries and aquaculture. *Climatic Change*, *177*(2), 26. https://doi.org/10.1007/s10584-024-03684-8

Kashkooli, O. B., Isfahani, P. M., & Modarres, R. (2025). Revisiting marine heatwaves baselines in warming oceans under nonstationary condition. *Science of the Total Environment*, *958*, 178194. https://doi.org/10.1016/j.scitotenv.2024.178194
Kauppi, L., & Villnäs, A. (2022). Marine heatwaves of differing intensities lead to distinct patterns in seafloor functioning. *Proceedings of the Royal Society B: Biological Sciences*, *289*(1986), 20221159. https://doi.org/10.1098/rspb.2022.1159
Keil, P., Mauritsen, T., Jungclaus, J., Hedemann, C., Olonscheck, D., & Ghosh, R. (2020). Multiple drivers of the North Atlantic warming hole. *Nature Climate Change*, *10*(7), 667–671. https://doi.org/10.1038/s41558-020-0819-8
Kirtman, B. P., Perlin, N., & Siqueira, L. (2017). Ocean eddies and climate predictability. *Chaos: An Interdisciplinary Journal of Nonlinear Science*, *27*(12), 126902. https://doi.org/10.1063/1.4990034
Li, M., Organelli, E., Serva, F., Bellacicco, M., Landolfi, A., Pisano, A., et al. (2024). Phytoplankton spring bloom inhibited by marine heatwaves in the north-western Mediterranean Sea. *Geophysical Research Letters*, *51*(20), e2024GL109141. https://doi.org/10.1029/2024GL109141
Li, X., Hu, Z., McPhaden, M. J., Zhu, C., & Liu, Y. (2023). Triple-Dip La Niñas in 1998–2001 and 2020–2023: Impact of mean state changes. *Journal of Geophysical Research: Atmospheres*, *128*(17), e2023JD038843. https://doi.org/10.1029/2023jd038843
Lubitz, N., Daly, R., Smoothey, A. F., Vianello, P., Roberts, M. J., Schoeman, D. S., et al. (2024). Climate change-driven cooling can kill marine megafauna at their distributional limits. *Nature Climate Change*, *14*(5), 526–535. https://doi.org/10.1038/s41558-024-01966-8
Martínez, J., Leonelli, F. E., García-Ladona, E., Garrabou, J., Kersting, D. K., Bensoussan, N., & Pisano, A. (2023). Evolution of marine heatwaves in warming seas: The Mediterranean Sea case study. *Frontiers in Marine Science*, *10*, 1193164. https://doi.org/10.3389/fmars.2023.1193164
Marullo, S., Serva, F., Iacono, R., Napolitano, E., Sarra, A. D., Meloni, D., et al. (2023). Record-breaking persistence of the 2022/23 marine heatwave in the Mediterranean Sea. *Environmental Research Letters*, *18*(11), 114041. https://doi.org/10.1088/1748-9326/ad02ae
Maturi, E., Harris, A., Mittaz, J., Sapper, J., Wick, G., Zhu, X., & Koner, P. (2017). A new high-resolution sea surface temperature blended analysis. *Bulletin of the American Meteorological Society*, *98*(5), 1015–1026. https://doi.org/10.1175/BAMS-D-15-00002.1
Merchant, C. J., Embury, O., Bulgin, C. E., Block, T., Corlett, G. K., Fiedler, E., et al. (2019). Satellite-based time-series of sea-surface temperature since 1981 for climate applications. *Scientific Data*, *6*(1), 223. https://doi.org/10.1038/s41597-019-0236-x
Minnett, P. J., Alvera-Azcárate, A., Chin, T. M., Corlett, G. K., Gentemann, C. L., Karagali, I., et al. (2019). Half a century of satellite remote sensing of sea-surface temperature. *Remote Sensing of Environment*, *233*, 111366. https://doi.org/10.1016/j.rse.2019.111366
Oliver, E. C., Benthuysen, J. A., Darmaraki, S., Donat, M. G., Hobday, A. J., Holbrook, N. J., et al. (2021). Marine heatwaves. *Annual Review of Marine Science*, *13*(1), 313–342. https://doi.org/10.1146/annurev-marine-032720-095144
Oliver, E. C. J., Donat, M. G., Burrows, M. T., Moore, P. J., Smale, D. A., Alexander, L. V., et al. (2018). Longer and more frequent marine heatwaves over the past century. *Nature Communications*, *9*(1), 1324. https://doi.org/10.1038/s41467-018-03732-9
Peal, R., Worsfold, M., & Good, S. (2023). Comparing global trends in marine cold spells and marine heatwaves using reprocessed satellite data. *State of the Planet*, *1-osr7*, 1–10. https://doi.org/10.5194/sp-1-osr7-3-2023
Pilo, G. S., Holbrook, N. J., Kiss, A. E., & Hogg, A. M. (2019). Sensitivity of marine heatwave metrics to ocean model resolution. *Geophysical Research Letters*, *46*(24), 14604–14612. https://doi.org/10.1029/2019GL084928
Schlegel, R. W., Darmaraki, S., Benthuysen, J. A., Filbee-Dexter, K., & Oliver, E. C. J. (2021). Marine cold-spells. *Progress in Oceanography*, *198*, 102684. https://doi.org/10.1016/j.pocean.2021.102684
Schoellhamer, D. H. (2001). Singular spectrum analysis for time series with missing data. *Geophysical Research Letters*, *28*(16), 3187–3190. https://doi.org/10.1029/2000gl012698
Sen Gupta, A. (2023). Marine heatwaves: Definition duel heats up. *Nature*, *617*(7961), 465. https://doi.org/10.1038/d41586-023-01619-4
Sen Gupta, A., Thomsen, M., Benthuysen, J. A., Hobday, A. J., Oliver, E., Alexander, L. V., et al. (2020). Drivers and impacts of the most extreme marine heatwave events. *Scientific Reports*, *10*(1), 19359. https://doi.org/10.1038/s41598-020-75445-3
Smith, K. E., Burrows, M. T., Hobday, A. J., King, N. G., Moore, P. J., Sen Gupta, A., et al. (2023). Biological impacts of marine heatwaves. *Annual Review of Marine Science*, *15*(1), 119–145. https://doi.org/10.1146/annurev-marine-032122-121437
Smith, K. E., Burrows, M. T., Hobday, A. J., Sen Gupta, A., Moore, P. J., Thomsen, M., et al. (2021). Socioeconomic impacts of marine heatwaves: Global issues and opportunities. *Science*, *374*(6566), eabj3593. https://doi.org/10.1126/science.abj3593
Smith, K. E., Gupta, A. S., Amaya, D., Benthuysen, J. A., Burrows, M. T., Capotondi, A., et al. (2024). Baseline matters: Challenges and implications of different marine heatwave baselines. *Progress in Oceanography*, 103404. https://doi.org/10.1016/j.pocean.2024.103404
Tanaka, K. R., & Houtan, K. S. V. (2022). The recent normalization of historical marine heat extremes. *PLOS Climate*, *1*(2), e0000007. https://doi.org/10.1371/journal.pclm.0000007
Thomas, N. P., Marquardt Collow, A. B., Bosilovich, M. G., & Dezfuli, A. (2023). Effect of baseline period on quantification of climate extremes over the United States. *Geophysical Research Letters*, *50*(17), e2023GL105204. https://doi.org/10.1029/2023GL105204
Wang, Y., Kajtar, J. B., Alexander, L. V., Pilo, G. S., & Holbrook, N. J. (2022). Understanding the changing nature of marine cold-spells. *Geophysical Research Letters*, *49*(6), e2021GL097002. https://doi.org/10.1029/2021GL097002
Xu, T., Newman, M., Capotondi, A., Stevenson, S., Di Lorenzo, E., & Alexander, M. A. (2022). An increase in marine heatwaves without significant changes in surface ocean temperature variability. *Nature Communications*, *13*(1), 7396. https://doi.org/10.1038/s41467-022-34934-x
Yang, C., Leonelli, F. E., Marullo, S., Artale, V., Beggs, H., Nardelli, B. B., et al. (2021). Sea surface temperature intercomparison in the framework of the copernicus climate change service (C3S). *Journal of Climate*, *34*(13), 5257–5283. https://doi.org/10.1175/JCLI-D-20-0793.1